Sensitivity Analysis of Adhesion in Computational Model of Elastic Doublet

Alžbeta Bohiniková[1(✉)], Iveta Jančigová[2], Ivan Cimrák[1,2], and James J. Feng[3]

[1] Research Centre, University of Žilina, 010 26 Žilina, Slovakia
Alzbeta.Bohinikova@rc.uniza.sk
[2] Cell-in-fluid Biomedical Modelling and Computations Group, Faculty of Management Science and Informatics, University of Žilina, 010 26 Žilina, Slovakia
[3] Department of Mathematics, University of British Columbia, Vancouver, BC V6T 1Z2, Canada
https://cellinfluid.fri.uniza.sk/

Abstract. This work introduces a computational model of elastic double cluster. We describe a method to create a partially flattened spherical cell and a mirroring process that creates a symmetrical double cluster with desired adhesion surface. The main focus is on the adhesion between the two cells modeled by repulsive-attractive Lennard-Jones potential. We study the stability of the adhesion with respect to the parameters of the Lennard-Jones potential and to the elasticity of the cells. Based on these, a baseline cluster is created and calibrated to a specific separation force using computational experiment that mimics a dual micropipette assay. This cluster is then immersed into elongation flow to create a parallel between the two types of cell stretching experiments: one that mechanically pulls the cell membrane and another where fluid flow creates stress on the membrane. Thus validated, our model of adhesion can be used in more complex clusters and serve as a building block in future computational studies.

Keywords: Computational model · Cell clusters · Adhesion · PyOIF

1 Introduction

The motivation to separate circulating tumor cell (CTC) clusters into individual cells arises from their higher metastatic potential [9] compared to the individual CTCs as well as their higher resistance to drugs [3]. To better understand how to break up the clusters, it is important to understand their bonds. There are experiments measuring such bonds in flow [17] or using micropippete aspiration [15]. There is also evidence that high shear stress [16] and specific drugs [4,5] can also help to break them apart.

I. Rojas et al. (Eds.): IWBBIO 2022, LNBI 13347, pp. 220–233, 2022.
https://doi.org/10.1007/978-3-031-07802-6_19

The work [17] investigates the separation force for clusters consisting of two cells. Using microfluidic chip with sudden narrow constriction they tested different flow conditions (by varying differential pressure in the microfluidic channel) and measured how many clusters separated. With the use of a computational model they determined that a separation force of $173\,nN$ is necessary to separate 50% of the clusters. Even at separation force $542\,nN$, there were 30% of clusters that did not separate. However, the range of the separation force varies across the literature, and the separation force measured by [17] is very much dependent on the channel design.

Other works look at the behaviour of cluster in various flow situations. A 2D liquid-drop model is used in [16] to represent single cells and doublets. In [1], [13], the clusters are modelled as one stiff mesh consisting of 2, 3 and 4 cells. A 3D elastic model is used to model clusters squeezing into a capillary sized channels in [2]. More detailed study about the adhesion of a single cluster cell to a microvasculature wall was performed in [7]. However, we could not find a study focused on the adhesion between individual cells.

In order to investigate this, we focus on a doublet of two identical cells. First, we briefly describe the model with details on modeling the adhesion bonds and contact surfaces. Then we focus on the pulling experiment (similar to optical tweezers experiment done with biological cells) and finally we consider a comparable elongation flow.

2 Computational Model of Double Cluster

2.1 Elastic Cells

Cell Model. The cells forming the cluster are modeled using a dissipative immersed boundary method [6] in 3D. The membrane is represented by a triangular mesh of nodes connected by elastic bonds. The five employed elastic moduli are stretching, bending, conservation of local area, conservation of global area and conservation of volume. The individual nodes are then coupled to the underlying lattice-Boltzmann model of the surrounding fluid. The model allows for viscosity contrast of the inner and outer fluid by using DPD particles inside the cell.

Cluster Model. While the individual (spherical) cells have a relaxed shape defined by their initial geometry and bonds of the mesh points, the cluster shape is determined by non-bonded interactions of points on neighboring membranes. As a consequence, the clusters may change shape and also the cells forming a cluster may separate. More information about the model and its implementation can be found at [18].

Cell Size. The size of the CTC varies depending on the type and stage of cancer and on the variation within the cell population. In [21] the cell line MDA-MB-231 has diameters $12.4 \mp 2.1\,\mu m$ (average of 128 cells) and the line MCF-10A has $11.2 \mp 2.4\,\mu m$ (average of 158 cells). For this work we chose cell diameter at the lower end of these ranges: $2r_{cell} = 10\ \mu m$.

Elastic Parameters. The original PyOif model [12] was calibrated for red blood cells (RBCs) using the optical tweezers data [11]. Qualitative observations [13] suggest that the elasticity of tumor cells can vary considerably, and as shown in e.g. [14], computational experiments are sensitive to the elastic parameters in the model. Considering that the CTCs are generally stiffer than RBCs [20], we have chosen the following moduli for our model cells: $k_s = 0.05\,\mu N/m$, $k_b = 0.005\,Nm$, $k_{al} = 0.02\,\mu N/m$, $k_{ag} = 0.7\,\mu N/m$, $k_v = 0.9\,\mu N/m^2$.

2.2 Adhesion

For the cells to create a cluster, they need to have an attractive force between them. However, the force cannot be only attractive, because computationally this would lead to cells collapsing onto each other. Real biological cells do not collapse but connect with bonds of small but finite length. To achieve this behaviour, we also need a repulsive force at very close range, that would prevent the cells from overlapping.

Lennard-Jones (LJ) potential is frequently used to model particle-particle interactions in coarse-grained simulations to represent interactions that are attractive at large distance and strongly repulsive at short distances [19]. Typically, in simulations it also has a cutoff distance and is only evaluated when the two particles (in our case a pair of points, one on each cell membrane) are closer than this cutoff distance. To calculate the LJ interaction energy one needs to consider the number of pairwise LJ interactions per square unit of membrane surface.

The potential is defined as:

$$V_{LJ}(r) = \begin{cases} 4\epsilon_{LJ}\left[\left(\frac{\sigma}{r}\right)^{12} - \left(\frac{\sigma}{r}\right)^{6}\right] & \text{if } r < r_{cut} \\ 0 & \text{otherwise} \end{cases} \tag{1}$$

where r is the distance between the interacting particles, r_{cut} is the cutoff distance and ϵ scales the strength of the interaction. The parameter σ determines the distance r_{min} where the repulsion changes to attraction. This switch occurs at the minimum of the potential, when $r = r_{min} = \sqrt{2}\sigma$.

Adhesion Surface. Two cells in a double cluster are adhered by a circular area with a given adhesion diameter. In double clusters images, e.g. in [9], the ratio between adhesion diameter and cell diameter is around 60%. So for our clusters we selected $r_{surf} = 3\,\mu m$ as a suitable radius of the spherical contact surface.

The typical shape of double cluster has two cells that are flattened at the contact surface. The yz plane is the plane of symmetry along which we flattened the cells. The points on the cells were selected to achieve the desired adhesion radius. And then the distance between the adhesion surfaces of the cells was set to r_{min}. The second cell was created as a mirror image of the first. This guarantees that we have pairs of points facing each other on the adhesion surface and with an appropriate choice of LJ parameters we can have each mesh point interacting

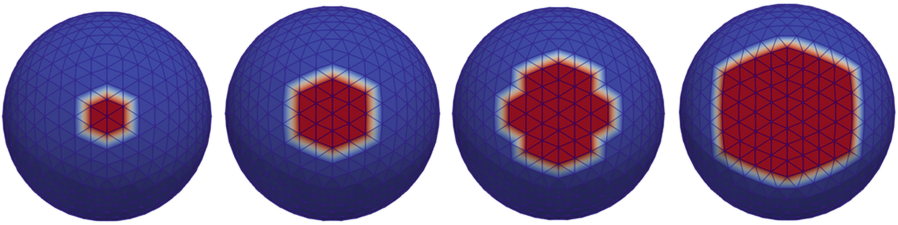

Fig. 1. Possible adhesion areas for baseline cluster with $k_b = 0.005\,Nm$, see Table 3.

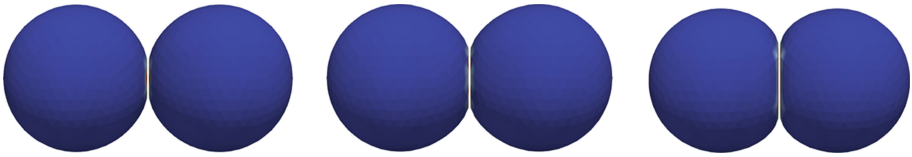

Fig. 2. Profiles of clusters with various adhesion areas shown in Fig. 1 for baseline cluster with $k_b = 0.005\,Nm$, see Table 3. Number of points on adhesion surface, from left to right: 19, 33, 61.

with exactly one mesh point of the other cell, which offers more control over the interaction and more stability of adhesion.

Adhesion Strength. Apart from the size of the surface, the strength of the adhesion is important, too. In [8], the authors used a micropippete aspiration method to measure the cell-cell adhesion strength of various human embryonic kidney cell clones, and determined them to be 2–12 nN. The cell-cell adhesion measurements in [15] give the separation force of mesoderm and endoderm cells in the range 2–5 nN. Based on these measurements we aimed to model a cluster with adhesion which separates under applied force between 1–2 nN. More specifically our baseline is a cluster that holds up to 1.5 nN and separates at 1.6 nN. We also discuss how we can change the cluster properties through the LJ interaction parameters to model other separation forces.

Stable Clusters. The clusters were created by putting two flattened and mirrored cells next to each other, flat sides facing, and applying the LJ interaction. We placed the cells at the equilibrium distance r_{min}, where there should be no LJ influence, provided that the only points in the interactions are the ones facing each other. This can be achieved by setting the parameters r_{min} and r_{cut} in such a way that the closest neighbour of the opposite point (considering the smallest edge length in the triangulation of the mesh) is further than r_{cut} and thus out of the range of the interaction. The clusters were then left to relax until the change of axial length of the cell was less than 0.01% per 10 μs.

It is important to note that even though the adhesion surfaces were set to be at the equilibrium of the LJ interaction, the relaxed distance between the cells was always slightly under r_{min}. This was expected, since the cells are elastic and

attempt to resume their original spherical shape. This pushes the points from the flattened area closer together. These points are then closer than r_{min} and the LJ interaction starts to repulse them. The final distance between the cells is then the distance where the forces are in balance.

2.3 Pulling Experiment

To determine the strength of the adhesion modeled with LJ potential we designed a simulation experiment mimicking the dual micropipette assay, such as the biological experiment in [8]. To achieve similar stretching, we pulled a cap of each cell with radius $2\,\mu m$. The pulling cap can be seen in Fig. 3. This size was selected as the most typical pipette radius [10].

Mirrored and flattened clusters were loaded into channels with static fluid that provides damping. The viscosity of the fluid was set to $1.5\,mPa\,s$. The simulation was run until the gap between the cells was larger than $1\,\mu m$, or until the cell stretched and the adhesion area stabilized, assuring that the cluster will not separate.

Using this experiment, we studied how individual parameters of cluster model influence the final behaviour of the cluster.

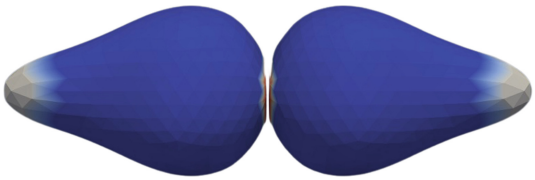

Fig. 3. Snapshot of cell deformation halfway through the pulling experiment. The white part of the mesh marks points to which the outward force is equally applied.

3 Stability of Adhesion Surface

Changes in parameters r_{min} and r_{cut} can improve the stability of the adhesion area. As shown in Table 1, the change to r_{min} does not influence the size of the stable area. For the same cell cluster we carried out a set of experiments where r_{min} was fixed and r_{cut} increased. As long as the r_{cut} was smaller than the distance to the second closest point on the opposite cell, the changes had no influence. This shows that the cell cluster with given elastic parameters, cell radius, mesh, adhesion area (represented by contact radius r_{surf} and number of mesh points shown in the final column of Table 1) and ϵ_{LJ} is stable. However, this stability changes if the elasticity of the cell changes.

Of the five employed elastic moduli, bending, which conserves angles between pairs of mesh triangles, is the most important modulus to the adhesion surface. In order to test how the changes in elasticity influence the stability of the adhesion, we tested changes in bending parameter k_b. With increased k_b, the cell becomes

Table 1. Contact radius r_{surf} does not depend on the size of the LJ repulsive region, with a set width of the attraction region of $0.15\,\mu m$ and other elastic and interaction parameters held constant (baseline cluster). The gap between the cells' flat adhesion surfaces is set to r_{min} (the actual gap is shown in column 3) and there is no other force applied to the cells. They are left to relax until the change in their axial length is less then 0.01% per $10\,\mu s$.

$r_{min}[\mu m]$	$r_{cut}[\mu m]$	gap $[\mu m]$	$r_{surf}[\mu m]$	points [-]
0.10	0.25	0.0999	3.08521	61
0.15	0.30	0.1497	3.08521	61
0.20	0.35	0.1994	3.08520	61
0.25	0.40	0.2491	3.08519	61
0.30	0.45	0.2988	3.08518	61
0.35	0.50	0.3484	3.08517	61

more rigid and resists the flattening of part of its surface more. Though the stable area changes only slightly, in Table 2 we can see that for $k_b \geq 0.02\,Nm$ the gap between the surfaces collapses and is no longer at r_{min}.

The gap is calculated as distance (in x-direction) between the leftmost point of the right cell and the rightmost point of the left cell, see also Fig. 4 for separation outcomes with a given elasticity and varying separation force. A negative gap represents the fact that the cells are overlapping. The contact area is still a flat surface, e.g. Fig. 2, but we see that higher pulling force leads to more prolonged cluster and smaller adhesion area.

Table 2. Influence of bending elasticity k_b on the stability of the adhesion radius r_{surf} and separation force F_s. **o** denotes a cluster that holds when the given force is applied. **x** denotes a cluster that separates when the given force is applied. Other elastic coefficients and interaction parameters are set to the baseline cluster. The gap between the cells' flat adhesion surfaces is set to r_{min} (the actual gap is shown in column 3). There is no other force applied to the cells. They are left to relax until the change in their axial length is less then 0.01% per $10\,\mu s$. Number of mesh points on the contact surface is in column 4.

$k_b[Nm]$	gap $[\mu m]$	$r_{surf}[\mu m]$	points[-]	F_s $[nN]$					
				1.3	1.4	1.5	1.6	1.7	1.8
0.000625	0.1499	3.1863	65	o	o	o	o	o	x
0.00125	0.1499	3.1864	65	o	o	o	o	o	x
0.0025	0.1498	3.1865	65	o	o	o	o	x	x
0.005	0.1497	3.0852	61	o	o	o	x	x	x
0.01	0.1485	3.0854	61	o	x	x	x	x	x
0.02	−0.1580	3.0812	61	x	x	x	x	x	x
0.04	−0.1585	3.0810	61	x	x	x	x	x	x

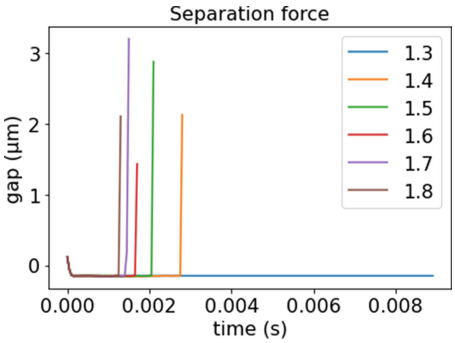

Fig. 4. Gap between cells for double cluster from Table 2 with $k_b = 0.01\,Nm$. Forces are given in $[n\,N]$. The abrupt ends of almost vertical lines represent the fact that the cluster has separated. The initial downward shift in all cases means that the starting gap was $0.15\,\mu m$ and at the beginning of the simulation the membranes crossed over and stabilized at distance $-0.15\,\mu m$.

The adhesion surface of more rigid cells is smaller than the one we have selected as the baseline and consequently more stable as shown in Table 3.

Table 3. Size of the adhesion area, represented by the number of points, depending on cells' elasticity and initial radius of the flattened surface. The stars note that the cells are overlapping.

$k_b[Nm]/r_{surf}[\mu m]$	0.5	1	1.5	2	3
0.000625	7	7	19	33	65
0.00125	7	7	19	33	65
0.0025	7	7	19	33	65
0.005	7	7	19	33	61
0.01	7	7	19	33	61
0.02	7	7	19*	29*	61*
0.04	7	7	19*	25*	61*

Adhesion strength parameter ϵ_{LJ} can be used to prevent cells from overlapping, but it also influences the magnitude of separation force necessary, see Table 4. With increasing ϵ_{LJ} the separation force F_s also increases.

To achieve more stable adhesion surface with gap at r_{min} levels, even if the cells are more rigid and the separation force kept at the desired level, a change in r_{min} and r_{cut} can help.

Table 5 shows that the first estimate for the value of ϵ_{LJ} (for mesh with 1182 points) was approximately $0.0036\,fNm$. This led to cluster separating even at the smallest separation force we tested, $F_s = 0.5\,nN$. As we can see in

Table 4. Separation force necessary for baseline cluster (642 mesh nodes per cell) depending on the adhesion parameter ϵ_{LJ}. The columns r_{surf}, *points* and *gap* show the stability of the adhesion surface when no external forces are applied. The LJ potential is set to $r_{min} = 0.15\,\mu m$ and $r_{cut} = 0.3\,\mu m$.

$\epsilon_{LJ}[fNm]$	gap$[\mu m]$	$r_{surf}[\mu m]$	points[-]	$F_s[nN]$				
				0.5	1.0	1.5	1.6	2.0
0.0025	0.14817	3.08517	61	o	x	x	x	x
0.005	0.14920	3.08520	61	o	o	x	x	x
0.0066	0.14968	3.08521	61	o	o	o	x	x
0.0075	0.14972	3.08521	61	o	o	o	o	x
0.01	0.14979	3.08521	61	o	o	o	o	o

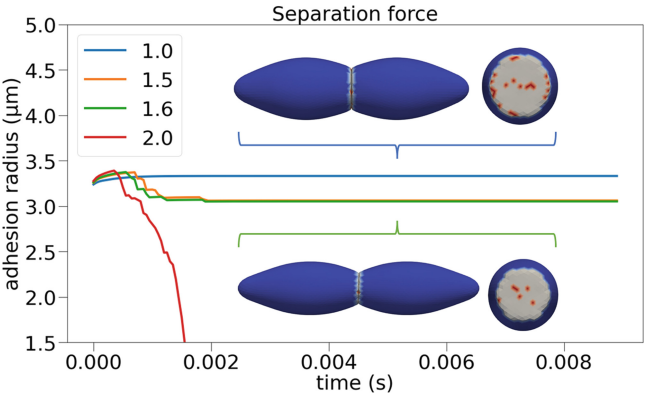

Fig. 5. Small variability in stabilized adhesion of clusters that do not separate, demonstrated using 1992 node cluster with LJ parameters $\epsilon_{LJ} = 0.005\,fNm$, $r_{cut} = 0.25\,\mu m$ and $r_{min} = 0.2\,\mu m$. The inset figures show profile and the adhesion area for pulling forces $1\,nN$ and $1.6\,nN$.

Table 7, to achieve F_s between $1.5\,nN$ and $1.6\,nN$, ϵ_{LJ} needs to be approximately $0.0065\,fNm$. This is in contrast to what can be seen for coarser discretization of our baseline cluster with 642 mesh points. The stability of the adhesion surface is not influenced by changing ϵ_{LJ}, as seen in Table 4, nor is it changed by moving r_{min} and r_{cut} as seen in Table 1.

For denser meshes, there is a higher risk of instability. This arises mainly from the interplay between the cell trying to achieve its original shape and the LJ interaction. During the initialization of the cluster, the cells are flattened, and positioned at distance r_{min}. In the next iteration step, some of the points on the flattened adhesion surface are pushed out, mainly by the bending interaction. This instantly puts them into the repulsive region of the LJ potential. Depending on how close they get to the second cell they are repulsed by a corresponding force, which pushes them into the attractive region of the LJ potential.

This fluctuation, stabilizes into either a gap less than r_{min} or above $-r_{min}$ (when the cells overlap), or the whole system diverges. By increasing r_{min} we allow for more space. So if we take similarly deformed meshes, the point (close to the border of the flattened surface) that is pushed into the repulsive region of LJ, is pushed with about the same force (since the deformation of the cell's surface is the same) for any value of r_{min} (since at the beginning the cells are r_{min} apart). However, with higher r_{min} the repulsive force given to this point is smaller and allows for more stable adhesion between cells.

Table 5. Stability of adhesion surface for 1182 node discretization.

simID	$\epsilon_{LJ}[fNm]$	$r_{min}[\mu m]$	$r_{cut}[\mu m]$	gap $[\mu m]$	$r_{surf}[\mu m]$	points [-]
1	0.0036	0.15	0.3	0.1474	3.36467	133
2	0.0060	0.15	0.3	−0.1337	3.36085	133
3	0.0060	0.15	0.25	−0.1404	3.36052	133
4	0.0060	0.2	0.3	0.1993	3.36467	133
5	0.0060	0.2	0.25	0.1993	3.36466	133

Thus, r_{min} should be set as small as possible to mimic the qualitative shape of biological cell clusters, whose membranes touch at the adhesion area, but large enough so that the adhesion is stable. The interaction cutoff r_{cut} should be set smaller than the distance of the point to its second closest neighbour on the opposite cell. If we set r_{cut} higher than this value, we could end up with one point being repulsed by one point but at the same time attracted by all six neighbours of this point, which would lead to instability. We calculated this threshold value for each mesh we used, see Table 6, as follows.

Since the cells are mirrored at the beginning, taking a pair of points facing each other from each cell and one of their closest neighbours, creates a right angle triangle. The distance between the opposing points is r_{min} and we estimate the distance between a point and its closest neighbour as the smallest edge length of our mesh e_{min} and then the maximum value for r_{cut} can be calculated as: $r_{cut_{max}} = \sqrt{r_{min}^2 + r_{cut}^2}$.

Baseline Cluster. As mentioned in previous sections, our baseline cluster has the following parameters: $r_{cell} = 5\,\mu m$, $r_{surf} = 3\,\mu m$, $k_s = 0.05\,\mu N/m$, $k_b = 0.005\,Nm$, $k_{al} = 0.02\,\mu N/m$, $k_{ag} = 0.7\,\mu N/m$, $k_v = 0.9\,N/m^2$. For discretization we selected a mesh with 642 points. LJ parameters were set to $r_{min} = 0.15\,\mu m$, $r_{cut} = 0.3\,\mu m$ and $\epsilon_{LJ} = 0.0066\,fNm$. r_{min} was selected the smallest possible to keep the cells from overlapping. r_{cut} was selected smaller than $r_{cut_{max}} = 0.62\,\mu m$, as calculated in Table 6 to have only one-to-one point LJ interaction on the adhesion surface, and then adjusted to achieve separation at 1.6 nN. ϵ_{LJ} was also tuned to achieve the desired separation force. This was done by running multiple parameter combinations in the pulling experiment. Similarly, we ran experiments

Table 6. Maximum value of r_{cut} for various discretisations. e_{min} e_{max} and e_{mean} denote minimal, maximal and mean edge.

$n_{nodes}[-]$	$e_{min}[\mu m]$	$e_{max}[\mu m]$	$e_{mean}[\mu m]$	$r_{min}[\mu m]$	$r_{cut_{max}}[\mu m]$
482	0.686	0.956	0.868	0.15	0.70
642	0.602	0.823	0.750	0.15	0.62
1182	0.332	0.779	0.556	0.2	0.39
1524	0.293	0.689	0.489	0.2	0.36
1922	0.338	0.480	0.434	0.2	0.39

for other mesh discretizations, see Table 7, to demonstrate consistent behavior across different levels of coarse-graining.

It is important to note that also values close to that stated in the table would lead to similar separation force. This would be valuable for more precise fine-tuning of the LJ interaction. This table should be used as a tool to initialise a cluster with similar behaviour as the baseline, only with different discretizations, that might be needed for simulations with more narrow channels.

4 Elongation Flow

To better mimic the microfluidic conditions, we also considered separation of double clusters in elongation flow. The flow is achieved by having the inflow at two opposite sides of the microfluidic chamber, as shown in Table 8, and outflow on two perpendicular sides. The cells are placed at the center in such a way that the contact area is perpendicular to the outflow. This way the flow drives the separation. The boundary inflow velocity is then adjusted to determine which velocities lead to separation and which are not strong enough.

Table 7. Various discretizations for baseline cluster. Values of r_{min} and r_cut were selected to achieve stable adhesion area with radius of 3 µm. ϵ_{LJ} was selected through series of pulling experiments with various forces and various values of ϵ_{LJ}. ϵ_{LJ} stated in the table results in clusters separating between 1.5 and 1.6 nN.

$n_{nodes}[-]$	$\epsilon_{LJ}[fNm]$	$r_{min}[\mu m]$	$r_{cut}[\mu m]$
482	0.0070	0.15	0.3
642	0.0066	0.15	0.3
1182	0.0065	0.2	0.25
1524	0.0060	0.2	0.25
1992	0.0048	0.2	0.25

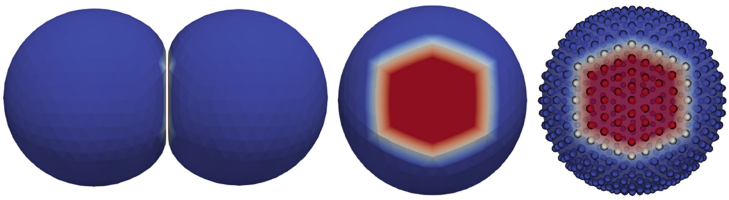

Fig. 6. Baseline cluster. The red points are at distance less than r_{min}, the white points are at distance between r_{min} and r_{cut}. (Color figure online)

Table 8. Validation of various discretization setting for the baseline cluster. The discretizations from Table 7 were used in elongation flow and exhibit consistent behavior: separating at inflow velocities 0.017 mm/s and above (x) and holding attached at inflow velocities 0.015 mm/s and below (o).

$n_{nodes}[-]$	$v_{inflow}[mm/s]$	
	0.015	0.017
482	o	x
642	o	x
1182	o	x
1524	o	x
1992	o	x

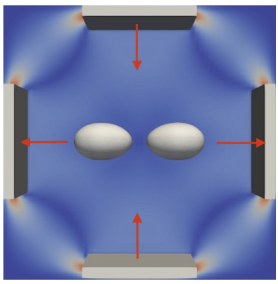

Using the cluster discretizations from Table 7 we determined the separation inflow velocity of elongation flow to be $\sim$0.016 mm/s (as measured at the center of the boundary, see Table 8).

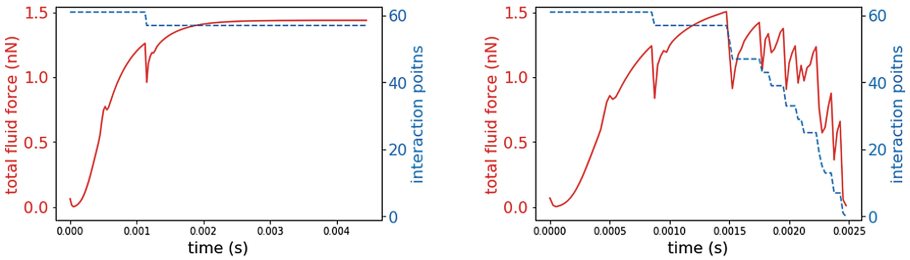

(a) $v = 0.015m/s$ (b) $v = 0.017m/s$

Fig. 7. Fluid force on cells in elongation flow. The red line indicates the fluid force acting on a cell at a given time, the blue dashed line shows number of points on the contact area. (a) no separation at lower fluid velocity (b) higher flow results in cluster separation. (Color figure online)

4.1 Fluid Force on Cell

To link the flow and force conditions needed to separate a given cluster, we measured the total fluid force acting on each cell in the elongation flow. This force has the same magnitude and opposite direction for the two cells and is calculated as a sum of fluid forces from all the individual mesh points, Fig. 7.

At lower applied fluid velocity in the elongation flow, Fig. 7 (a), we see an increase in the total fluid force as the cell membrane stretches and thus moves relatively to the surrounding fluid. The sharp jump corresponds to the moment when the contact area decreases (some of the bonded pairs no longer hold). The fluid force on the object then equalizes with the adhesion force and the system is at equilibrium.

At larger applied fluid velocity in elongation flow, Fig. 7 (b), we see a similar initial increase in the total fluid force, followed by multiple sharp jumps. Each of these corresponds to the contact area decreasing (blue line), when some of the bonded points no longer hold. Before the fluid force has a chance to equalize with the adhesion force another jump occurs, ultimately leading to cell separation. At that point the total fluid force is 0, indicating both cells are moving with the fluid.

While the correspondence is not perfect (most likely due to numerical reasons), we see that a cluster that separates at 1.5–1.6 nN pipette pulling force, holds at $\sim$1.4 nN fluid pulling force and separates around 1.5 nN. This means we can use the total acting fluid force as a proxy when evaluating the strength of adhesion in flow.

5 Conclusion

The adhesion area and its stability depend on many factors. With increased cell rigidity, represented by higher values of the bending parameter, the adhesion surface becomes less stable, especially for larger contact surfaces. We have shown that to a certain extent this instability can be managed by appropriate settings of the LJ potential parameters. To increase the stability, the repulsion/attraction threshold r_{min} can be increased, which leads to fewer fluctuations. The increase of ϵ_{LJ} can also improve the stability of the relaxed adhesion surface, however it is directly proportional to the adhesion strength.

To satisfy the need for various dicretizations of cell membrane, we have calibrated our baseline cluster for five meshes of various densities. Based on these, appropriate parameters for other meshes can be reasonably interpolated. The values in Table 7 suggest that to achieve the same behaviour of the cluster with an increased number of nodes, ϵ_{LJ} must be lowered and if the stability requires it, r_{min} increased and r_{cut} adjusted accordingly. We have explained and calculated the upper boundary for the value of r_{cut}, see Table 6.

This setup allows us to simulate any type of double cluster with varying elasticity, adhesion strength and adhesion surfaces. Building on this, more complex clusters can be explored, with higher number of cells and varying cell sizes.

Another direction of future work is to look at the behavior of this type of cluster under different flow conditions, such as in shear flow, parabolic flow or more complex flows with other types of cells. We have shown the first step in this direction with the elongation flow and determining the flow velocity that corresponds to the separation force in the pulling experiment.

Acknowledgements. This research was supported by Operational Program "Integrated Infrastructure" of the project "Integrated strategy in the development of personalized medicine of selected malignant tumor diseases and its impact on life quality", ITMS code: 313011V446, co-financed by resources of European Regional Development Fund.

This work was also supported by the Slovak Research and Development Agency (contract number APVV-15-0751).

James J. Feng acknowledges support by the Natural Sciences and Engineering Research Council of Canada (Discovery Grant No. 2019-04162).

References

1. Anderson, K.J., de Guillebon, A., Hughes, A.D., Wang, W., King, M.R.: Effect of circulating tumor cell aggregate configuration on hemodynamic transport and wall contact. Math. Biosci. **294**, 181–194 (2017)
2. Au, S.H., et al.: Clusters of circulating tumor cells traverse capillary-sized vessels. Proc. Natl. Acad. Sci. **113**(18), 4947–4952 (2016)
3. Bithi, S.S., Vanapalli, S.A.: Microfluidic cell isolation technology for drug testing of single tumor cells and their clusters. Sci. Rep. **7**(1), 1–12 (2017)
4. Bonnet, J., et al.: Mitotic arrest affects clustering of tumor cells. Cell Div. **16**(1), 1–13 (2021)
5. Choi, J.W., Kim, J.K., Yang, Y.J., Kim, P., Yoon, K.H., Yun, S.H.: Urokinase exerts antimetastatic effects by dissociating clusters of circulating tumor cells. Can. Res. **75**(21), 4474–4482 (2015)
6. Cimrák, I., Jančigová, I.: Computational Blood Cell Mechanics, 1st edn. CRC Press, Boca Raton (2018)
7. Dabagh, M., Gounley, J., Randles, A.: Localization of rolling and firm-adhesive interactions between circulating tumor cells and the microvasculature wall. Cell. Mol. Bioeng. **13**(2), 141–154 (2020)
8. Daoudi, M., et al.: Enhanced adhesive capacities of the naturally occurring ile249-met280 variant of the chemokine receptor cx3cr1. J. Biol. Chem. **279**(19), 19649–57 (2004)
9. Edd, J.F., et al.: Microfluidic concentration and separation of circulating tumor cell clusters from large blood volumes. Lab Chip **20**(3), 558–567 (2020)
10. Hochmuth, R.M.: Micropipette aspiration of living cells. J. Biomech. **33**(1), 15–22 (2000)
11. Jančigová, I., Kovalčíková, K., Bohiniková, A., Cimrák, I.: Spring-network model of red blood cell: From membrane mechanics to validation. Int. J. Numer. Meth. Fluids **92**(10), 1368–1393 (2020)
12. Jančigová, I., Kovalčíková, K., Weeber, R., Cimrák, I.: Pyoif: computational tool for modelling of multi-cell flows in complex geometries. PLOS Comput. Biol. **16**(10), 1–21 (2020)

13. King, M.R., et al.: A physical sciences network characterization of circulating tumor cell aggregate transport. Am. J. Physiol. Cell Physiol. **308**(10), C792–C802 (2015)
14. Kovalcikova, K., Bachraty, H., Bachrata, K., Buzakova, K.: Numerical experiment characteristics dependence on red blood cell parameters, pp. 286–292 (2021)
15. Maître, J.L., et al.: Adhesion functions in cell sorting by mechanically coupling the cortices of adhering cells. Science **338**(6104), 253–256 (2012)
16. Marrella, A., et al.: High blood flow shear stress values are associated with circulating tumor cells cluster disaggregation in a multi-channel microfluidic device. PLoS ONE **16**(1), e0245536 (2021)
17. Mutlu, B.R., et al.: In-flow measurement of cell-cell adhesion using oscillatory inertial microfluidics. Lab Chip **20**(9), 1612–1620 (2020)
18. PyOIF: Computational Tool for Modelling of Multi-Cell Flows in Complex Geometries: Resources webpage for pyoif. online January 2022. https://cellinfluidfriunizask/resources-espresso/
19. Rapaport, D.C.: The Art of Molecular Dynamics Simulation, 2nd edn. Cambridge University Press, Cambridge (2004)
20. Shaw Bagnall, J., Byun, S., Begum, S.E.A.: Deformability of tumor cells versus blood cells. Sci Rep **5**(1), 1–11 (2015)
21. TruongVo, T., et al.: Microfluidic channel for characterizing normal and breast cancer cells. J. Micromech. Microeng. **27**(3), 035017 (2017)